Evaluating the performance of an operational infrasound avalanche detection system at three locations in the Swiss Alps during two winter seasons

Stephanie Mayer[a],[*], Alec van Herwijnen[a], Giacomo Ulivieri[b],[c], Jürg Schweizer[a]

[a] *WSL Institute for Snow and Avalanche Research SLF, Davos, Switzerland*
[b] *iTem s.r.l. - Integrated Technologies for Environmental Monitoring, Florence, Italy*
[c] *GeCo s.r.l., Florence, Italy*

ARTICLE INFO

ABSTRACT

Avalanche occurrences are unambiguous indicators of unstable snow conditions. Information on past and current avalanche activity is therefore crucial for avalanche forecasting. To continuously assess avalanche activity, automatic detection systems are required. In recent years, technological and signal processing advances have led to the development of operational infrasound avalanche detection systems. We evaluated the detection performance of four operationally running infrasound detection systems installed at three different sites in the Swiss Alps during two entire winter seasons. To this end, we collected a comprehensive data set of avalanche activity using a network of automatic cameras and supplementary field observations by local observers. The events automatically identified by the systems were then compared to the data set of visually observed avalanches. Only 3% of the 839 observed avalanches were associated with automatic detections and 21% of the automatic detections were confirmed by field observations. However, the majority of observed avalanches were small and most automatic detections occurred during periods of poor visibility. Furthermore, the probability of detection (POD) increased with avalanche size, decreased with distance, and varied with avalanche type. Dry-snow avalanches were generally better detected than wet-snow and mixed-type avalanches. Large avalanches (on the order of 300 m wide and 1000 m long) within a distance of 3 km from the array were typically well detected (POD ≈ 90%). The false alarm ratio was estimated to 13–30%.

1. Introduction

Avalanche forecasting and risk management strongly depend on the availability of information on the snowpack and its instability. Since the occurrence of avalanches provides an unambiguous indicator for unstable snow conditions, avalanches are considered as good predictors for further avalanches (e.g., McClung and Schaerer, 2006; Schweizer et al., 2012). Exact knowledge about the time and location of avalanche events is therefore crucial for regional as well as local forecasting. An increase in avalanche activity might indicate the time to close a road. Also, the decision to re-open the road is facilitated if the frequency of avalanches decreases. Consequently, timely information on the temporal evolution of avalanche activity can reduce risk and closing times.

Monitoring avalanche activity simply by visual observation is not sufficient. The visibility of relevant avalanche paths is particularly limited during periods of heavy snowfall, when timely data on avalanche occurrences are particularly wanted. There is thus a need for remote detection systems, which enable real-time monitoring of avalanche activity in a specific area independent of visibility.

Currently, three different technologies exist for the automatic remote detection of avalanches: infrasonic sensors (e.g. Marchetti et al., 2015; Schimmel et al., 2017; Scott et al., 2007; Thüring et al., 2015), ground based and satellite radar sensors (e.g. Eckerstorfer et al., 2016; Gauer et al., 2007; Schimmel et al., 2017) as well as seismic sensors (e.g., Heck et al., 2018; Lacroix et al., 2012). Among these types of detection systems, radar and infrasound systems are currently used operationally (e.g. Johnson et al., 2018; Koschuch, 2018; Persson et al., 2018; Steinkogler et al., 2018). While radar systems can detect even small avalanches on predefined adjacent avalanche paths (Persson et al., 2018; Schimmel et al., 2017; Steinkogler et al., 2016), infrasound detection is not restricted to a certain avalanche path as long as the avalanche to be detected reaches a certain size (Schimmel et al., 2017; Steinkogler et al., 2016; Thüring et al., 2015).

Infrasound technology is based on the detection of low-frequency

---

(< 20 Hz) longitudinal pressure waves propagating through the air at speed of sound and has been used to monitor artificial processes such as explosions (Ceranna et al., 2009) as well as various natural phenomena such as volcanic activity (Ripepe et al., 2007), debris flows (Kogelnig et al., 2014) and avalanches. Avalanches produce infrasound as the flowing and turbulent snow masses create pressure fluctuations in the air (Bedard Jr. et al. 1988; Kogelnig et al., 2011; Naugolnykh and Bedard Jr, 2002). The discovery of avalanche-generated infrasound by Bedard Jr. et al. (1988) and the subsequent development of infrasound systems for avalanche detection (Chritin et al., 1997; Scott et al., 2007; Ulivieri et al., 2011) also contributed to avalanche dynamics research. For example, recent studies (Havens et al., 2014; Marchetti et al., 2015) used infrasound detection systems to calculate avalanche velocities. Moreover, Kogelnig et al. (2011) combined seismic and infrasound detection methods to identify different avalanche flow regimes. The authors concluded that infrasound sensors are more sensitive to the turbulent snow-air flow (powder cloud) of an avalanche, while seismic sensors are more suitable to detect the dense flow at the lower avalanche path.

As the attenuation of infrasound in the atmosphere is low, infrasonic waves can travel over large distances from tens (Marchetti et al., 2016) to thousands (Fee et al., 2013) of km. Hence, infrasound detection systems can potentially record avalanches releasing many kilometers away from the sensors. The small atmospheric attenuation of infrasonic waves, however, leads to a great amount of infrasonic noise arriving at the sensors, both from natural (e.g. wind, earthquakes) and human (e.g. traffic, industrial activity) sources. Recent advances in infrasound technology have facilitated the discrimination between signal and noise. In particular, the use of arrays consisting of multiple sensors deployed in a particular geometry has enhanced the identification of signals generated by avalanches compared to single sensor systems (Scott et al., 2007; Ulivieri et al., 2011). Array processing techniques allow filtering out ambient noise signals (e.g. from wind) that arrive at the different sensors in a mutually uncorrelated manner. Nevertheless, avalanche signals must be distinguished from correlated signals originating from other infrasound sources such as aircrafts. A common method to separate avalanche events from non-events consists in applying threshold-based criteria on signal features such as pressure amplitude, direction of incidence and event duration (Marchetti et al., 2015; Ulivieri et al., 2011). These threshold-based classifiers reduce the number of false alarms, but can also lead to smaller or more distant avalanches not being detected automatically, even if their infrasound signal reaches the sensors (Steinkogler et al., 2016).

Infrasonic sensor arrays have been reported to be capable of detecting small- to medium-sized avalanches at distances of up to 3–4 km away from the sensor system (Hendrikx et al., 2018; Humstad et al., 2016; Thüring et al., 2015; Ulivieri et al., 2011) and large avalanches at distances of up to 14 km (Steinkogler et al., 2016). Wet-snow avalanches are believed to be more challenging to detect than dry-snow avalanches, as they typically flow with slower velocities and therefore produce less infrasound (e.g., Kogelnig et al., 2011). However, to the best of our knowledge, no comprehensive study exists yet that investigates in detail the performance and limitations of infrasound detection systems in dependence on avalanche size, type and distance to the sensors.

Our objective was therefore to assess the performance of infrasound avalanche detection systems with a special focus on avalanche size, type and source-to-receiver distance. We compared automatically detected events to natural avalanche activity data obtained by visual observations at three different sites throughout the Swiss Alps (Goms, Frutigen and Quinto) during the entire winter seasons 2015–2016 and 2016–2017. For the visual survey of avalanche activity, a network of automatic cameras was used and supplemented with detailed field observations by local observers.

2. Methods

2.1. Setup and signal processing

The infrasound monitoring systems known as IDA (Infrasound Detection of Avalanches) consisted of four- or five-sensor infrasound arrays with a triangular geometry and an aperture, i.e. the maximum distance between two elements, of approximately 150 m. The array elements were equipped with differential pressure transducers, with a sensitivity of 200 mV Pa^{-1} in the frequency band 0.01–100 Hz and low self-noise (-62 dB Pa^2 Hz^{-1}, relative to 1 Pa). Pressure data were recorded at a sampling rate of 50 Hz with a 16-bit digitizer and GPS time synchronization. Digital data from the peripheral sensors were transmitted through fibre-optic cables to the central element of the array where data were synchronized, stored and transmitted via modem to a server which processed the data in near-real time.

To discriminate signal from noise, a multi-channel correlation method was combined with windowing (windows of 5 s with 0.5 s overlap). The infrasonic wave parameters of the incoming signal determined by means of the multi-channel correlation method included the apparent velocity (the sound propagation speed within the plane defined by the elements of the array and directly reflecting the elevation of the infrasonic source) and the back-azimuth angle of the detected signal (i.e. the angle between the direction of incidence of the wave emanating from the signal source and the north direction) (for details see Marchetti et al., 2015).

Starting from the series of contiguous (0.5 s) infrasonic events resulting from windowing, threshold criteria were applied to automatically discriminate signals generated by avalanches from other natural (e.g. earthquakes, meteors, thunder) and anthropogenic (e.g. traffic, explosions, industry) infrasonic events. The criteria for the automatic detection of infrasonic signal produced by avalanches were based on the assumption that an avalanche is a moving source of infrasound (Marchetti et al., 2015) and included four main thresholds. Two thresholds were related to the kinematics defining the degree of migration of the apparent velocity and the back-azimuth over time, whereas the other two were related to the size of the event: minimum duration and peak amplitude of the signal (Table 1). The choice of the duration threshold (1, Table 1) refers to the minimum signal duration that allows a characterization of the moving source as avalanche flow and consequently indicates the limit of the method for small avalanches. With the choice of an upper amplitude threshold (2, Table 1), we aimed at avoiding false alarms linked to anthropogenic and natural (e.g. microbaroms) sources. The apparent velocity criterion (3, Table 1) reflects the movement from top to bottom, while the back-azimuth migration criterion (4, Table 1) is linked to the azimuth rotation of the moving source. The latter depends on the relative positions of the avalanche paths with respect to the array and therefore must be chosen site-specifically. We optimized the corresponding back-azimuth threshold value for each site based on recordings of confirmed events. For duration, amplitude and apparent velocity migration index, the thresholds were the same for each site. If an event met all of the four threshold criteria, it was classified as an avalanche with "high" reliability. An event meeting the minimum duration criterion as well as two of the three other criteria (2, 3, or 4 in Table 1) was rated as an avalanche with "medium" reliability. An alarm was automatically sent via

Table 1

Threshold criteria for automatic detection of avalanches.

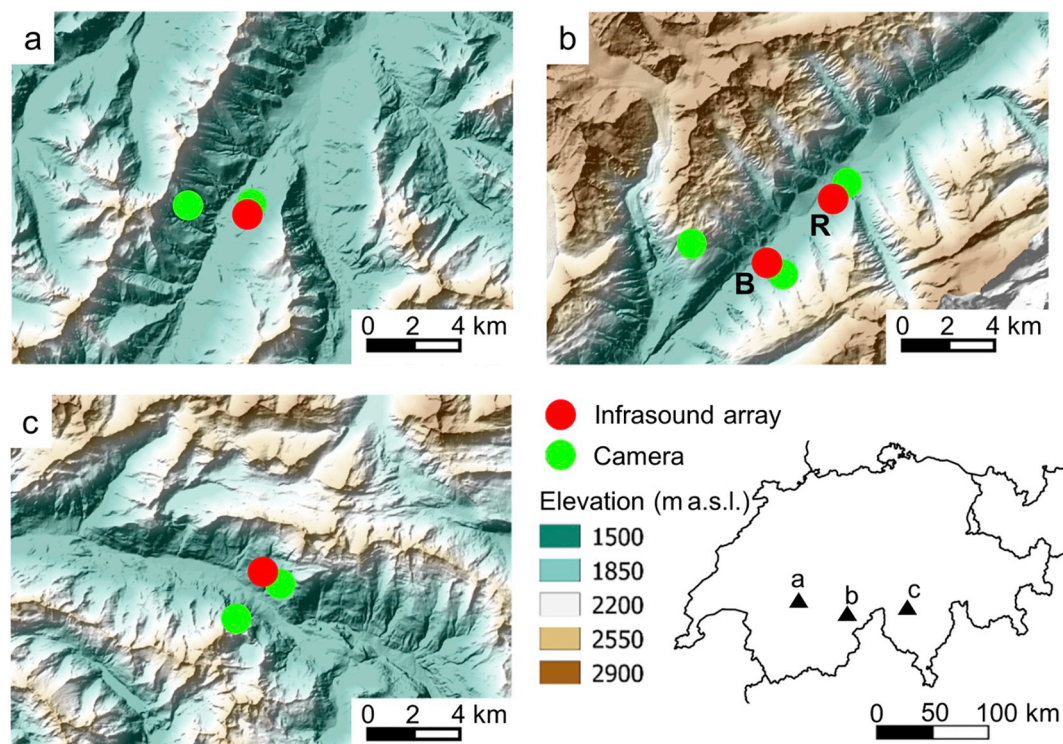| Criterion		Threshold
1	Minimum duration	> 20 s
2	Minimum amplitude	> 0.1 Pa
3	Apparent velocity migration index	< −30%
4	Back-azimuth migration index (%)	*site specific*

Fig. 1. Overview of the three sites: (a) Frutigen, (b) Goms (B: Blitzingen, R: Reckingen) and (c) Quinto with positions of infrasound systems (red dots) and cameras (green dots). The map at the bottom right of the figure indicates the location of the sites within Switzerland. (For interpretation of the references to colour in this figure legend, the reader is referred to the web version of this article.)

text message (SMS) to local avalanche safety personnel when an event with "high" reliability was detected. In the following, we will use the term detections for events that were automatically identified as potential avalanches with either high or medium reliability.

2.2. Sites

A total of four infrasound arrays were installed at three different sites in the Swiss Alps (Fig. 1). One infrasound system was deployed at 1340 m a.s.l. in the Engstligen valley close to Frutigen (Bernese Oberland). Relevant release areas are located on both sides of the valley at elevations of up to 2600 m a.s.l. The second site was located in the valley of Goms (Valais), where two systems were installed in order to monitor the mountain ranges on both sides of the valley rising up to >3000 m a.s.l. Both arrays were installed at the bottom of the valley, the first one near Blitzingen at 1310 m a.s.l. and the second one 4.5 km further northeast near Reckingen at 1330 m a.s.l.

The fourth array was installed in the Valle Leventina (Ticino) at 1340 m a.s.l. close to Quinto. Here, potential starting zones extend up to 2700 m a.s.l. and especially the NNE-facing avalanche paths opposite of the system endanger highway and settlements below.

2.3. Visual survey of avalanche activity

For visual monitoring of avalanches, we installed at least two automatic camera systems at each site to record images in various directions every 10 min. The images from the automatic cameras were available online in near real-time and covered most of the relevant avalanche paths. The visual identification of avalanches on the images was influenced by the weather and daytime dependent visibility conditions as well as by the local topography and the degree of vegetation at the respective site. At the site of Frutigen for instance, the large proportion of forest-free, open areas provided a good view into relevant release areas and runout zones. At the sites of Goms and Quinto, on the

other hand, a more complex topography and denser forestation partly concealed some avalanche paths. To record avalanches not visible on the images and to obtain more complete observations, local observers regularly performed field surveys. Due to site-dependent differences in the accessibility of avalanche-prone areas, the quality and completeness of the avalanche activity data recorded by the local observers differed between sites.

All avalanches observed on the images or by local observers were mapped in a GIS tool. This data set was also supplemented by avalanche events extracted from the ProTools database, which is an operational information system (Pertschy et al., 2016) enabling local avalanche safety services in Switzerland to record avalanches on a topographic map. We included all avalanches within a radius of 10 km around the respective infrasound system to determine whether detections originated from distant avalanches.

Based on the observational data, we derived several parameters for each of the mapped avalanches. As an indicator for the size of the avalanche, we used the projections of its mapped area onto the plane. For each avalanche observed on the images of the cameras, we determined a plausible timespan for its release by identifying the time interval between the last picture with sufficient visibility and without the avalanche and the first picture on which the avalanche was seen. This time interval was at least 10 min and in case of poor visibility sometimes extended to several days. Likewise, we took into account an uncertainty in the time of release of the avalanches recorded by local observers but not visible on the images of the automatic cameras. This uncertainty was determined by the amount of time with poor visibility, again determined from the images from the automatic cameras, before the date the avalanche was observed.

We further classified all avalanches with mapped areas larger than 10^4 m^2 into the three categories wet, dry and mixed (i.e. dry snow in the upper avalanche path and wet snow in the runout) to investigate the influence of the avalanche type on the probability of detection. Usually, the distinction between dry-snow and wet-snow avalanches is based on

the failure process in the starting zone (e.g. Baggi and Schweizer, 2009; Mitterer and Schweizer, 2013). For the purpose of this study, we were only interested in the flow characteristics of the avalanches, as this affects the production of infrasound. To classify an avalanche as either wet or dry, we therefore considered whether the flow behavior of the avalanche was dominated by wet or dry snow. This differentiation was based on visual characteristics in the runout zone (e.g. "dirty" parts with "snow-ball structure" typical for wet-snow) observed on the images of the automatic cameras. For avalanches with characteristics of wet-snow flow behavior in the runout zone, we in addition assessed the characteristics at starting zone elevation by consulting the air temperature measurements from nearby weather stations. In case of rather dry-snow conditions in the starting zone, we classified these avalanches as mixed-type.

2.4. Verification analysis

The data set of infrasound detections contains the exact time, signal duration, initial, final and average values of the back-azimuth angle as well as the associated reliability information for each detection. To analyze the effectiveness of the infrasound system, we compared the data set of automatic detections to the set of observed avalanches at the corresponding site and calculated various performance measures based on a 2 × 2 contingency table (Table 2).

With the definitions and abbreviations used in the contingency table (Table 2), the probability of detection (POD), the false alarm ratio (FAR) and the probability of non-events (PON) are defined as follows (Wilks, 2011):

Probability of detection: $\quad POD = \dfrac{H}{H + M}$ (1)

False alarm ratio: $\quad FAR = \dfrac{FA}{FA + H}$ (2)

Probability of non-events: $\quad PON = \dfrac{CN}{CN + FA}$ (3)

A high-performance system is characterized by a high POD value (ideal score: 1), while maintaining a high PON (ideal score: 1) and a low FAR (ideal score: 0), thereby identifying avalanche occurrences and the absence of avalanches equally well.

Since some avalanches might have been missed in the visual observations especially during periods of bad visibility, the number of events in the categories correct non-events (CN) and false alarms (FA) can only be estimated and not be determined with high confidence. For example, not every detection that could not be allocated to an avalanche can be considered as a false alarm, as it might relate to a visually not observable avalanche. For the same reason, the number of misses (M) and hits (H) are uncertain, and the uncertainty can even not be quantified. Nevertheless, we determined estimates for each of the three scores (POD, FAR, PON) based on the criteria described below.

2.4.1. Probability of detection

A pair of automatic detection and observed avalanche was counted as a hit, if all of the three following conditions were fulfilled:

Table 2
2 × 2 contingency table as used to calculate performance measures (compare Eqs. (1)–(3)).

		Visual observations	
		Non-avalanche event	Avalanche event
Automatic infrasound detection	Non-event	Correct non-events (CN)	Misses (M)
	Event	False alarms (FA)	Hits (H)

1. The time of detection lies within the period in which the avalanche was presumed to have occurred.
2. The azimuth angle corresponding to the start of the detected signal lies within ±10° of the azimuth angle corresponding to the starting zone of the observed avalanche.
3. The sign of the azimuth angle migration, i.e. the sign of the difference between final and starting value of the azimuth angle indicating the direction of movement of the signal source, corresponds to the path of the observed avalanche.

Initial and final values of the azimuth angle do not necessarily correspond to starting and runout zone of the avalanche, but rather mark the part of the avalanche path on which infrasound was generated. Therefore, we introduced a tolerance range of ±10° for the initial value of the azimuth angle in the second condition, which also accounts for uncertainties in the mapping of the avalanche. As different avalanche paths can be described with the same azimuth values, the matching between infrasound detections and observed avalanches was not always straightforward, especially if several avalanches occurred from a similar azimuthal range during a major snow storm. Moreover, the uncertainties inherent in the observational data (e.g. lacking information on the exact time of the avalanche occurrence) translate to the matching process as well. Therefore, a non-quantifiable uncertainty in the matching process inherently exists. All observed avalanches that could not be allocated to any detection according to the above criteria were counted as misses.

Since the performance of an infrasound detection system can be assumed to depend on its distance to the avalanche path as well as on the avalanche size, we calculated the POD in dependence of these parameters. We therefore grouped all avalanche events, represented by the pair of values $(A, D) := $ (mapped area, distance to the nearest infrasound system), into different size and distance classes. For each area-distance class defined by an area range $[A_1, A_2]$ and a distance range $[D_1, D_2]$, the respective probability of detection (POD) was calculated as proportion of detected avalanches among all observed avalanches in that particular class, i.e.

$$POD([A_1,A_2],[D_1,D_2]) := \frac{\text{number of hits with } (A,D) \in [A_1,A_2] \times [D_1,D_2]}{\text{number of all hits and misses with } (A,D) \in [A_1,A_2] \times [D_1,D_2]}$$ (4)

To assess how POD values change with avalanche size, we also defined the cumulated $POD_{cum,\ [D_1,D_2]}$ for three different distance ranges, providing, for each value A of the mapped avalanche area, the POD for events with mapped area larger than A and distances in the fixed interval $[D_1, D_2]$, i.e.

$$POD_{cum,[D_1,D_2]}(A) := POD([A,\infty],[D_1,D_2])$$ (5)

2.4.2. False alarm ratio

If no avalanche matched a detection, we examined whether it was a false alarm. Each unconfirmed detection was therefore allocated to one of the following categories:

a) *Unrealistic signal:* The combination of initial and final value of the azimuth angle do not fit to any avalanche path. For example, the initial azimuth value ±10° matches a potential release zone, but the final azimuth value would imply an upward flow of the avalanche.
b) *Good visibility:* Visibility on the day of or after the detection was good, but no avalanche was observed at the potential location indicated by the azimuth angle.
c) *Bad visibility and low danger:* Visibility on the day of and after the detection was poor, but an avalanche was very unlikely due to rather stable snow conditions (avalanche danger level "1-Low" or "2-Moderate").
d) *Bad visibility and high danger:* Visibility of relevant avalanche paths on the day of and after the detection was limited and a natural

avalanche was likely, given the rather unstable snow conditions at the time (avalanche danger level "3-Considerable" or higher).

Clearly, a single detection can fall into two of these categories. We decided to assign a detection to the first suitable category, considering the order a-b-c-d. Assigning an unconfirmed detection to either the category (b) or (c) indicates that it was likely a false alarm. Unconfirmed detections allocated to category (a) are likewise potential false alarms. Based on these categories, a conservative estimate for the false alarm ratio was calculated as

$$\text{FAR:} = \frac{\text{number of unconfirmed detections in a, b, c}}{\text{number of all detections}} \qquad (6)$$

However, there is a certain chance that anomalies in the signal characteristics arose from topographic barriers between the avalanche and the array. A lower bound for the false alarm rate was hence determined by only taking into account the detections in (b) and (c), i.e.

$$\text{FAR}_{\text{low}}: = \frac{\text{number of unconfirmed detections in b, c}}{\text{number of all detections}} \qquad (7)$$

It should be noted that some of the detections in (d) may also have been false alarms and thus may lead to a higher value of the false alarm ratio than that estimated according to Eq. (6).

2.4.3. Probability of non-events

To determine the PON, we only took into account days with good visibility and no avalanches, such that the possibility of missing an avalanche in the visual observations could be excluded. For the days with good visibility, which were manually identified based on the pictures of the automatic cameras, we defined PON_{gv} as follows:

$$\text{PON}_{\text{gv}}: = \frac{\text{number of days with good visibility, no avalanche observation and no detection}}{\text{number of days with good visibility and no avalanche observation}}$$

$$(8)$$

This definition is based on Eq. (3) using a time resolution of one day for the parameters CN and FA.

3. Results

3.1. Seasonal overview

In both winter seasons 2015–2016 and 2016–2017, snow depth was mostly below average (Fig. 2). During both winter seasons 2015–2016 and 2016–2017, a total of 672 avalanches of all sizes were visually observed in the 10 km surrounding of the four infrasound systems. For the analysis of detection performance, we took into account that every avalanche at the Goms site might have been detected by both infrasound systems (Blitzingen and Reckingen, Fig. 3). Therefore, avalanches that occurred within a 10 km-radius of both of these systems were counted twice in the performance analysis. Moreover, we excluded all avalanches that occurred during times when the corresponding infrasound system was out of order. In total, the number of avalanche events that were relevant for the analysis amounted to 839 (Table 3).

The four infrasound systems provided a total of 110 automatic detections and 23 (or 21%) of these automatic detections were associated with visually observed avalanches. Thus, only 3% of the visually observed avalanches were automatically detected by one of the infrasound systems. However, the probability of detection strongly depended on avalanche size and source-to-receiver distance, as explained in more detail in Section 3.2. Distinguishing between high reliability (4 criteria fulfilled) and medium reliability detections (only 3 criteria fulfilled), most hits (16 out of 23) corresponded to high reliability detections, although these make up only 41 of the 110 detections.

Fig. 2 shows a comparison between the number of observed avalanches (upper histogram) and the number of automatic detections (lower histogram) for each day of the two measurement periods without an explicit matching between detections and visual observations. These plots do not display the uncertainty in the release time of the observed avalanches, which amounted to more than one day in some cases. Instead, each event was plotted at the date belonging to the end of the possible time interval of release, meaning that some of the observed avalanches could have released earlier than indicated. Despite the uncertainty in the actual release times of the observed avalanches, the comparison of observations and automatic detections shows that not every peak of detections corresponded to a peak of observations and vice versa.

Overall, the majority of observed avalanches were small (Fig. 4). In fact, around two thirds of the 839 relevant events had a mapped area of $<10^4$ m^2. A large portion of the observed avalanches were either wet-snow or mixed-type avalanches due to warm temperatures. Among the avalanches with areas $>10^4$ m^2, about 43% were dry-snow avalanches, while the percentage of wet-snow or mixed-type avalanches was about 28% each (Fig. 4).

The best agreement between observations and detections was found for an avalanche cycle at the Goms site in the beginning of March 2017, when it rained up to 2400 m a.s.l after heavy snowfall and many large avalanches with mapped areas of the order of 1 km^2 were observed. These events were mostly classified as mixed-type since they released as dry-snow slab avalanches, whereas the deposit consisted of wet snow. The peak of observations during this prominent avalanche cycle coincided with a pronounced peak in the automatic detections by the infrasound system in Blitzingen (Fig. 2). In general, the highest number of detections was produced by the system in Blitzingen during the 2016–2017 season and almost half of these 32 detections were matched with visually observed avalanches (Table 3). Unfortunately, the second system (Reckingen) at the Goms site was out of operation during this time as a thick ice layer had formed above one of the infrasound sensors.

Among all sites and measurement seasons, most avalanches were visually observed in Frutigen during the 2016–2017 winter season. However, the majority of these events were small avalanches and glide-snow avalanches, such that 91% of the in total 244 observed events had a mapped area of $<10^4$ m^2 (Table 3). In this season, observations and detections did not match (Fig. 2). At the site of Quinto, only a few avalanches ($N = 6$ in 2015–2016 and $N = 10$ in 2016–2017) were observed in both winter seasons and none of these avalanches were assigned to any of the 10 automatic detections (Fig. 2, Table 3).

3.2. Probability of detection

To analyze the probability of detection in terms of avalanche size and source-receiver distance, we grouped all observed avalanche events, represented by the pair of values $(x, y) := (\text{mapped area}, \text{distance to the nearest infrasound system})$, into four size classes and three distance classes (Fig. 5). For each of the resulting 12 area-distance classes (Fig. 5a), we calculated the corresponding POD according to Eq. (4).

Small avalanches (A $< 10^4$ m^2), accounting for 67% of the observational data set, were not detected at all and only a small fraction (POD = 11%) of the medium-sized avalanches ($10^4 \leq$ m$^2 <$ A $< 10^5$ m^2) within a radius of 3 km were detected. On the other hand, large avalanches (A $\geq 10^5$ m^2) within a distance of 3 km from the array were well detected (POD = 88%).

The continuous increase of the cumulative $\text{POD}_{\text{cum}, [D_1, D_2]}$ (defined in Eq. (5)) with avalanche size for fixed ranges of distance (0 to 3 km and 3 to 10 km) is shown in Fig. 5b. The resulting two curves should be considered as indicative only, since they strongly depend on the underlying set of data points which become sparse with increasing mapped area. The increase in the cumulative POD with avalanche size was nearly linear for avalanches with mapped areas smaller than 10^5 m^2. For larger avalanches, the increase was no longer linear and more erratic (not shown), as the number of avalanches was rather limited (8
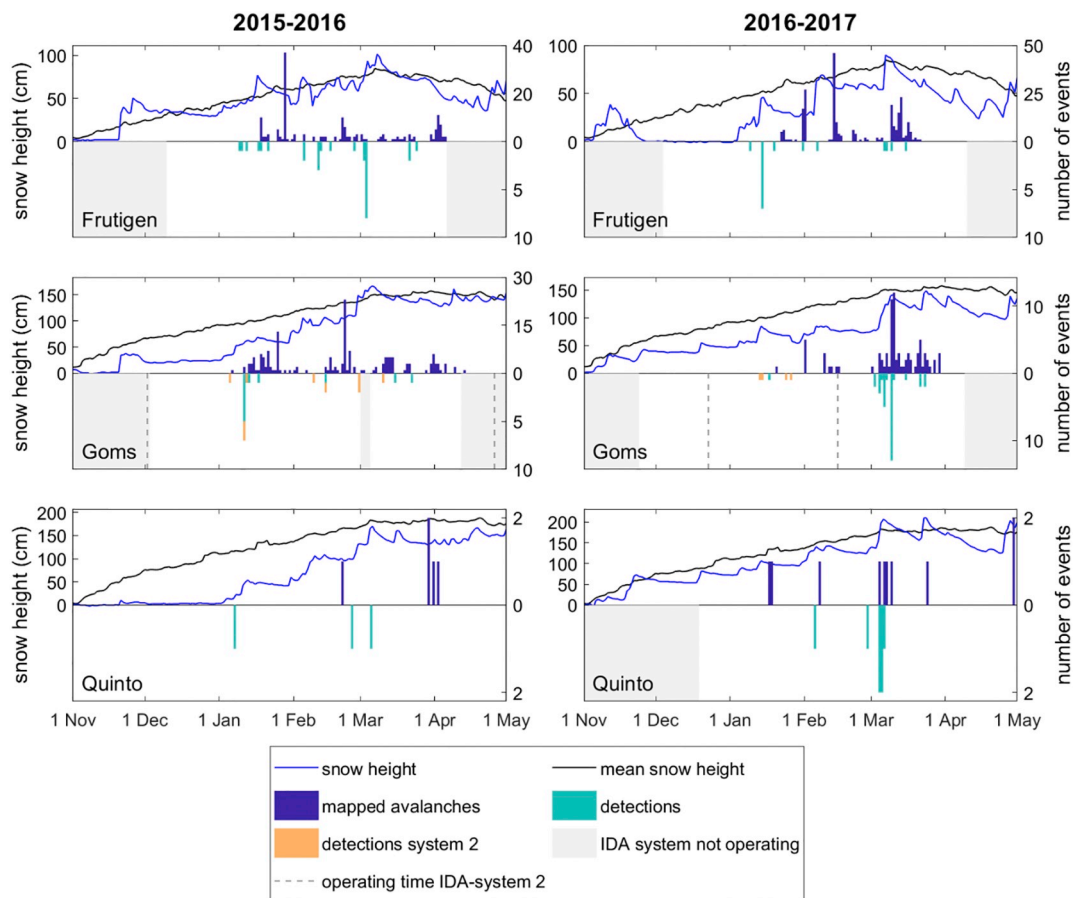
Fig. 2. Seasonal overview for each site (rows) and both winter seasons (columns) showing a daily comparison of observed avalanches (blue bars, upper half, second y-axis) and detections (green bars, lower half, second y-axis). At the Goms site (Fig. 3), a second infrasound system was operating (orange bars) during the time period in between the grey dashed lines. Non-operating periods of all other infrasound systems are indicated by grey coloring. Moreover, the snow height measured at automatic weather stations in the vicinity of the infrasound arrays (measured in ten minute intervals) as well as the mean snow height over 18 years at the same weather stations are displayed in the upper part (left y-axis) of the respective plot. (For interpretation of the references to colour in this figure legend, the reader is referred to the web version of this article.)

for D < 3 km and 7 for 3 < D < 10 km, respectively). For avalanches within a distance of 3 km, the POD increased more prominently than for avalanches at distances larger than 3 km.

Among the 278 medium-sized and large avalanches, a total of 23 events were detected. Different types of avalanches were detected, namely 12 dry-snow, 2 wet-snow and 8 mixed-type avalanches as well as one glide-snow avalanche (medium-sized, A = 12,000 m², D = 4.4 km). The most distant dry-snow avalanche that was still detected released >6 km away from the array (A = 27,000 m²), while the

most distant and still detected wet-snow and mixed-type avalanches in the same size class (medium-size) released at distances below 3 km. In the size category of large avalanches, the most distant detected avalanche was a mixed-type avalanche that occurred at a distance of almost 6 km. The most distant large dry-snow and wet-snow avalanches occurred at distances of 3 km and 2 km, respectively, to the nearest array, but there were also no undetected large avalanches of the same types releasing further away than these two events. A calculation of distinct POD values for each of the three avalanche types was not
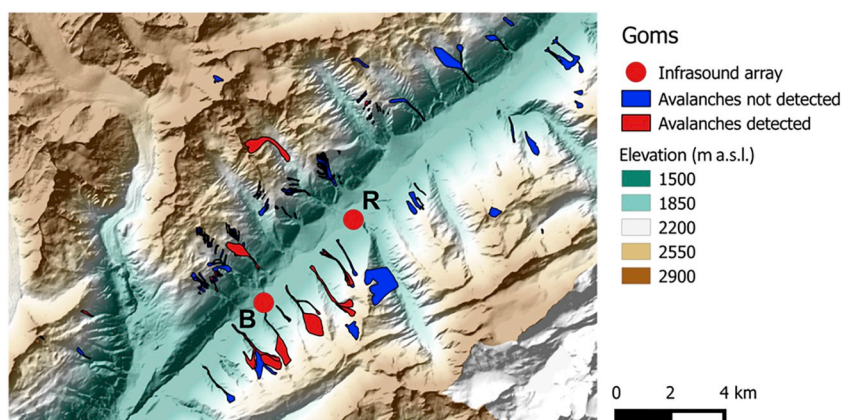

Fig. 3. Observed avalanches of both winter seasons at the Goms site. The red polygons indicate the avalanches detected by at least one of the two infrasound arrays (red dots, B: Blitzingen, R: Reckingen), while blue polygons display avalanches that were not detected by any of the systems. (For interpretation of the references to colour in this figure legend, the reader is referred to the web version of this article.)

Table 3

Numbers of visually observed avalanches (in brackets: percentage of avalanches with mapped area smaller than $10^4 \, m^2$), numbers of automatic infrasound detections (in brackets: number of high reliability detections among these) and number of hits (in brackets: number of high reliability detections among these) for all sites and both measurement seasons. The hits were determined according to the criteria described in section 2.4 above.

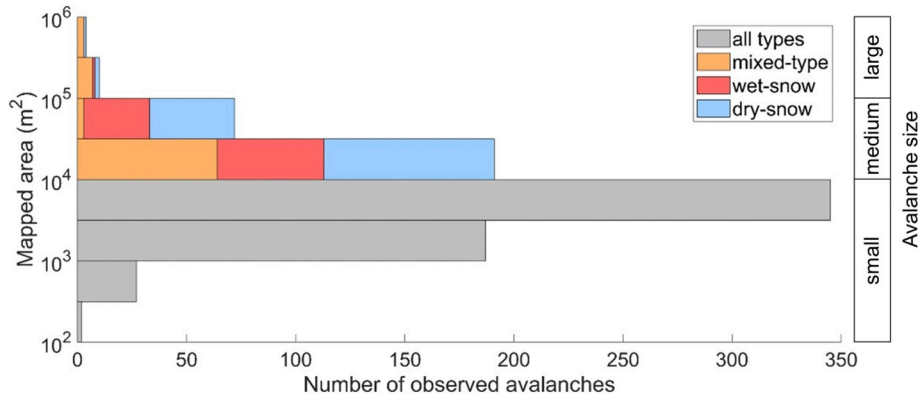|	Observed avalanches (mapped area < $10^4 \, m^2$)		Detections (high reliability)		Hits (high reliability)	
	2015–2016	2016–2017	2015–2016	2016–2017	2015–2016	2016–2017
Frutigen	164 (35%)	244 (91%)	27 (10)	15 (5)	3 (2)	0 (0)
Goms: Blitzingen	164 (75%)	74 (26%)	13 (5)	32 (16)	2 (1)	14 (10)
Goms: Reckingen	166 (75%)	11 (63%)	9 (3)	4 (1)	4 (3)	0 (0)
Quinto	6 (100%)	10 (30%)	3 (0)	7 (1)	0 (0)	0 (0)
Total	500 (62%)	339 (74%)	52 (18)	58 (23)	9 (6)	14 (10)
Total 2015–2017	839 (67%)		110 (41)		23 (16)	

Fig. 4. Distribution of mapped area for all observed avalanches ($N = 839$). For avalanches with mapped areas larger than $10^4 \, m^2$, the avalanche type is specified (orange: mixed-type, red: wet-snow, blue: dry-snow), while smaller avalanches are displayed without differentiation between types (grey bars). (For interpretation of the references to colour in this figure legend, the reader is referred to the web version of this article.)

feasible, as in the uppermost size range, data were limited to only a few avalanches per type. For example, only eight large avalanches ($A > 10^5 \, m^2$) were observed at distances <3 km. Thereof, six were classified as mixed-type avalanches and one each as dry-snow and wet-snow avalanche. With the exception of one mixed-type avalanche, all avalanches of this size-distance-class were detected. For medium-sized avalanches at distances of <3 km, where sufficient data points were available (82 avalanches), a differentiation between avalanche types resulted in a POD of 19% for dry-snow and a POD of only 4% for wet-snow or mixed events. Based on the latter result, we expect the POD for large dry-snow avalanches at distances of <3 km, of which we have only one example in our data set, to exceed the average POD value (88%) for all three types in this size-distance class.

3.3. False alarm ratio and probability of non-events

Overall, the infrasound systems produced 110 detections. Only about every fifth detection was attributed to an observed avalanche (Fig. 6). Of course, we cannot simply classify the remaining 87 unconfirmed detections as false alarms, since they may have originated from avalanches which could not be observed on the pictures of the automatic cameras or by the local observers. Either poor visibility, new snow covering the avalanche, or the remoteness of the avalanche path may have hindered the visual observation. Yet, we can estimate the FAR, i.e. the number of false alarms over the number of all detections, by considering the classification of unconfirmed detections into the four categories defined in section 2.4 above and using Eqs. (6) and (7).
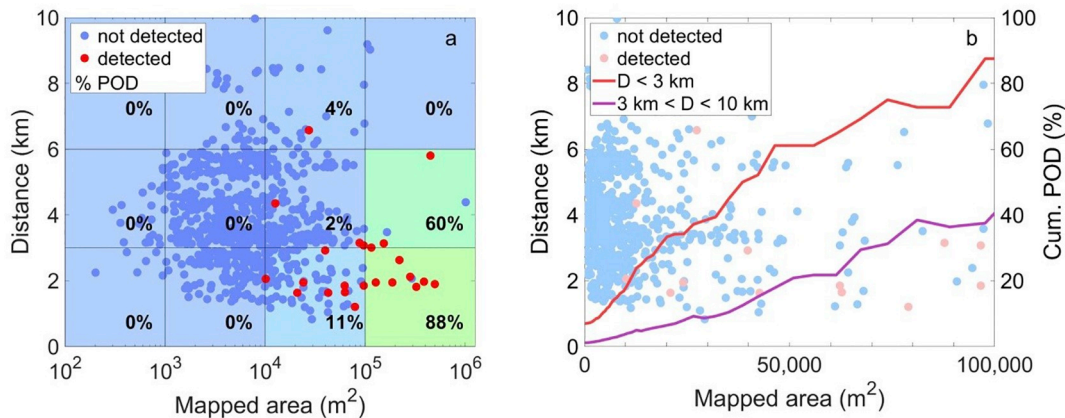

Fig. 5. (a) Hits (i.e. detected events, red dots, $N = 23$) and misses (i.e. undetected events, blue dots, $N = 816$) among all observed avalanches ($N = 839$) as function of projected area (x-axis, logarithmical scale) and distance to the nearest infrasound system (y-axis). Numbers (in %) indicate the POD for a particular area-distance class (rectangles); the POD is also visualized by the colors of the rectangles (green: high POD, blue: low POD). (b) Cumulated $POD_{cum, \, [D_1, D_2]}$ (in %) for avalanches at distances of <3 km (red curve) and >3 km (purple curve) to the nearest infrasound system as a function of the projected area (right y-axis). The dots again represent the observed events as a function of projected area (x-axis, now linear scale) and distance (left y-axis). (For interpretation of the references to colour in this figure legend, the reader is referred to the web version of this article.)
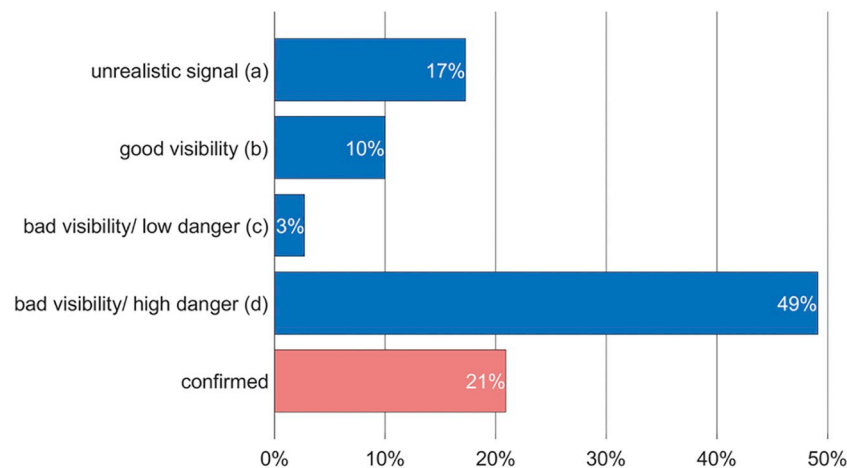
Fig. 6. Characteristics of detections. For the unconfirmed detections (blue bars) the four categories (a-d) as defined above are given (N = 110). (For interpretation of the references to colour in this figure legend, the reader is referred to the web version of this article.)

Considering categories (a), (b) and (c) (unrealistic signal characteristics; good visibility and bad visibility and low danger) yielded a FAR of 30%. Still, some of the detections in category (d) (bad visibility and high danger), which make up almost half of all detections, could be false alarms as well. Hence, the true FAR might as well be higher than 30%. On the other hand, anomalies in the signal characteristics may occur from topographic barriers between the avalanche and the array (category (a)). A lower bound FAR_{low} can thus be estimated as 13% by only considering the detections in categories (b) and (c) (Eq. (7)). Among the 33 detections in categories (a), (b) and (c), 10 were "high reliability" detections.

Over all sites and both winter seasons, we identified 172 days when no avalanche was observed and visibility conditions were ideal, i.e. the likelihood of missing an avalanche in the visual observations was very low. In this set of selected days, we found 9 days on which automatic infrasound alarms (in category (a) or (b)) were produced. This results in a PON_{gv} value (Eq. (7)) of 95%.

4. Discussion

We evaluated the performance of infrasound systems with observations of avalanche activity in their surroundings. Using visual observations to assess the performance of a detection system that is intended to provide better information on avalanche activity than conventional visual observations clearly poses a challenge. Although we recorded avalanche activity using a network of automatic cameras and information from detailed field observations by local observers, our visual avalanche catalogue most likely lacks avalanches released during periods of poor visibility or in out-of-sight avalanche paths. This may have resulted in overestimated POD values, as the number of avalanches that were not detected by the infrasound system may be higher. On the other hand, some of the unconfirmed automatic detections could have originated from avalanches not included in the visual survey, leading to an underestimation of POD values and an overestimation of the FAR. However, we found that only medium-sized to large avalanches were automatically detected, and it is questionable that numerous of these avalanches were missed by local observers or on images from the automatic cameras. This is particularly true for the Frutigen site where avalanche paths are visible from the road. Nevertheless, unconfirmed detections corresponding to avalanche paths that were not visible during or shortly after the time of detection were excluded from the calculation of the FAR in order to avoid an overestimation.

A further difficulty arose from the uncertainty in the release time of avalanches observed after periods of bad visibility. In particular, the matching of events during the major avalanche cycle at the beginning of March 2017 at the site of Goms was challenging, since numerous avalanches released at similar azimuthal ranges. To overcome these uncertainties in future studies, several infrasound arrays should be deployed at the same site within a few kilometers distance (< 3 km), such that the exact avalanche path can be inferred from the overlapping of the different azimuthal ranges. At the Goms site, two infrasound arrays were installed at a distance of 4.5 km, but unfortunately the second system malfunctioned during the main avalanche cycle in March 2017.

We analyzed the probability of detection in terms of avalanche size and source-receiver distance and found large avalanches to be well detected within a distance of 3 km from the system. The most distant avalanche in the uppermost size range ($>10^5$ m^2) that was still detected released almost 6 km away from the infrasound array and was classified as mixed-type avalanche. However, more data points are needed to assess the detection performance for large avalanches at distances of >3 km from the system. The overall low POD (<4%) for medium-sized avalanches at distances >3 km suggests that large avalanches might likewise not be reliably detected beyond 3 km. At this distance range attenuation, distortion as well as shading effects due to near-source topography on the acoustic wave field produce ambiguous infrasonic wave parameters strongly reducing the capability of automatic detection (Lacanna and Ripepe, 2013). For example, the overall largest avalanche (mixed-type), observed at the site of Goms at a distance of around 4 km to the array of Blitzingen, was not detected by this system, presumably due to the large mountain ridge in between (Fig. 3). The second system at this site (Reckingen) was out of operation at the time of release.

The degree of sound diffraction by a topographic barrier depends on its relative size with respect to the acoustic wavelength (Hadden Jr. and Pierce, 1981; Lacanna and Ripepe, 2013). The main mountain ranges delimiting the alpine valleys of the three sites and extending to a multiple of the relevant acoustic wavelengths produce strong attenuation as well as diffraction phenomena that reduce the resolution of the apparent velocity migration and therefore the effectiveness of the kinematic thresholds (Table 1). For this reason, only avalanches within the valley can be identified automatically. Conversely, the smaller topographical barriers within the main valleys that compare with the acoustic wavelength in size are negligible for wave propagation and thus allow the automatic detection of avalanches at paths not in direct sight with respect to the system. Within the main valley, however, the resolution of the apparent velocity migration is reduced with distance. Although large avalanches at distances >3 km from the system are in some cases identifiable in the signal, the performance of the automatic detection method is strongly restricted. Also the fact that only 3 out of

13 automatic detections produced by the second infrasound system (Reckingen) at the site of Goms coincided with automatic detections from the first system (Blitzingen), supports the finding that the detection performance is rather low for distances above 3 km, since the two systems are around 4.5 km apart from each other.

Our results support the findings of previous studies, which also stated that the detection of small avalanches is not possible, whereas large avalanches are well detected (Schimmel et al., 2017; Steinkogler et al., 2016; Steinkogler et al., 2018; Thüring et al., 2015). Interestingly, a recent study that evaluated the same infrasound system over one winter season at Rogers Pass, British Columbia, Canada (Hendrikx et al., 2017) suggested that even avalanches of size 1.5 (Canadian size classification) can be detected within a distance of 4 km. This finding contrasts with our result that none of the numerous observed avalanches with an area smaller than 10^4 m^2 were automatically detected. However, Hendrikx et al. (2017) also stated that an operational system should be able to detect size 1.5 to 2 avalanches within a range of 1.5 km distance. Our data set mainly includes avalanches that released >1.5 km away from the infrasound system. For medium-sized to large avalanches, Hendrikx et al. (2017) postulate a limiting range of 3 km source-to-receiver distance for reliable detection performance (POD > 0.8) based on their investigations that took into account all avalanches within 5 km and within line-of-sight of the infrasound system. This supports the hypothesis that the limiting range of 3 km determined in our analysis represents a technical limitation of infrasound technology rather than being determined by local topographic features. We therefore assume that the 3 km limit also applies to other locations as long as there are no major topographic barriers in between the infrasound array and the avalanche paths.

Moreover, for medium-sized avalanches and distances smaller than 3 km, the POD for dry-snow avalanches was about five times higher than for wet-snow and mixed avalanches. This finding supports the assumption that the infrasound detection of wet-snow avalanches is less reliable than the detection of dry-snow avalanches. Past studies about infrasonic signals generated by avalanches (Kogelnig et al., 2011; Naugolnykh and Bedard Jr, 2002) concluded that the main source of infrasound energy is the turbulent snow-air flow part of the avalanche (powder cloud). Therefore, significantly lower pressure amplitudes and hence lower POD values are expected for wet-snow avalanches than for dry-snow avalanches. On the other hand, we found that among the large avalanches at distances of <3 km, five (out of six) visually observed mixed-type avalanches and one (out of one) wet-snow event were automatically detected. The duration of the detected signal exceeded one minute for most of these events. As for these type of events it is unlikely that powder clouds were involved over a major part of the flow, we conclude that a turbulent snow-air flow component is not a prerequisite for the automatic infrasound detection. We assume that even in the absence of powder clouds, the acceleration of snow masses can act as detectable source of infrasound, provided that the avalanche path is steep enough and the avalanche volume is sufficiently large. Nevertheless, seismic array systems (Heck et al., 2019a; Lacroix et al., 2012) appear to be the better choice when focusing on the detection of wet-snow avalanches since seismic sensors are more sensitive to vibrations generated by dense flow regimes (Kogelnig et al., 2011). In the future, a combination of infrasonic and seismic arrays could shed further light on the processes involved in the production of infrasound signals by different types of avalanches. In this context, Heck et al. (2019a) recently showed that also seismic arrays can resolve infrasound waves depending on the array geometry.

Our estimation of the FAR (13–30%) significantly differs from other studies conducted in Canada (Hendrikx et al., 2017) and Norway (Humstad et al., 2016), where it was estimated at almost 0%. An explanation for this deviation might be the relative remoteness of the sites in Canada and Norway compared to the more congested Swiss valleys. Also, the relatively thin snow cover over the infrasound sensors at the Swiss sites during both test winters may have favored the occurrence of false alarms produced by anthropogenic noise, a common problem also in seismic avalanche detection (Heck et al., 2019b).

Following Marchetti et al. (2015), we used four threshold criteria to automatically detect avalanches. These simple criteria should effectively filter out the short and weak signals generated by natural and anthropogenic sources of infrasound. On the other hand, the application of these threshold criteria limited the detection capability to large avalanches within a distance of about 3 km from the array. The automatic detection of more distant and smaller avalanches could be enabled by applying less stringent threshold criteria. Such an adjustment of the underlying threshold values would, however, come at the cost of an increased FAR. An alternative to the threshold-based classification of events are machine-learning approaches that statistically optimize the classification process (e.g. Heck et al., 2019b; Thüring et al., 2015). Future studies should investigate how these compare to the threshold-based classification applied in our study.

5. Conclusions

We evaluated the detection performance of four operational infrasound detection systems (IDA) over two entire winter seasons (2015–2016, 2016–2017). By comparing 110 automatic IDA detections to 839 visually observed avalanches, we found that the probability of detection increased with avalanche size and decreased with source-receiver distance as expected. Large avalanches (> 10^5 m^2) within a distance of around 3 km from the array were typically well detected (POD about 90%). The data set of large detected avalanches in this distance range included dry-snow, wet-snow and mixed-type avalanches. On the other hand, the detection probability of medium-sized avalanches ($10^4 \leq m^2 < A < 10^5$ m^2) was rather low (POD = 19% for dry-snow and POD = 4% for wet-snow and mixed-type avalanches at distances smaller than 3 km). Small avalanches (< 10^4 m^2), which made up the majority (67%) of our verification data set, were not detected at all. Evaluating the false alarm ratio was not straightforward as periods of poor visibility did not allow the verification of more than half of the automatic detections. A qualitative estimate of the false alert ratio ranges between 13% and 30%.

Overall, our results show that in the absence of major topographic barriers to the propagation of infrasound waves, infrasound avalanche detection systems are well suited to reliably monitor large dry-snow and mixed-type avalanches up to a distance of about 3 km and are also able to detect large wet-snow avalanches in this distance range. Infrasound detection systems can thus provide important additional information for local avalanche safety services during major avalanche cycles. In future studies, the effect of topographic barriers on the detection performance should be investigated, for instance by deploying several infrasound systems at one site. Moreover, more data should be gathered to distinguish between dry-snow and wet-snow avalanches when calculating detection rates for large avalanches.

Author contribution statement

JS and AvH initiated and designed the study. AvH and SM were responsible for the installation and maintenance of the camera systems, GU for the infrasound systems. SM analyzed the data, GU contributed to the analyses. SM prepared the manuscript with contributions from all co-authors.

Declaration of Competing Interest

SM, AvH and JS declare they have no conflict of interest. GU was involved in the development of the operational infrasound system and its commercialization.

Acknowledgements

References

Baggi, S., Schweizer, J., 2009. Characteristics of wet snow avalanche activity: 20 years of observations from a high alpine valley (Dischma, Switzerland). Nat. Hazards 50 (1), 97–108.

Bedard Jr., A.J., 1989. Detection of avalanches using atmospheric infrasound. In: Proceedings of the 57th Annual Western Snow Conference. Colorado State University, Fort Collins CO, U.S.A, pp. 52–58 18–20 April 1989.

Bedard Jr., A.J., Greene, G.E., Intrieri, J., Rodriguez, R., 1988. On the Feasibility and Value of Detecting and Characterizing Avalanches Remotely by Monitoring Radiated Sub-Audible Atmospheric Sound at Long Distances, Proceedings of a Multidisciplinary Approach to Snow Engineering, July 11–14 1988. Santa Barbara, CA, pp. 267–275.

Ceranna, L., Le Pichon, A., Green, D.N., Mialle, P., 2009. The Buncefield explosion: a benchmark for infrasound analysis across Central Europe. Geophys. J. Int. 177 (2), 491–508.

Christin, V., Rossi, M., Bolognesi, R., 1997. Acoustic detection system for operational avalanche forecasting. In: Proceedings International Snow Science Workshop, Banff, Alberta, Canada, 6–10 October 1996. Canadian Avalanche Association, Revelstoke BC, Canada, pp. 129–133.

Eckerstorfer, M., Bühler, Y., Frauenfelder, R., Malnes, E., 2016. Remote sensing of snow avalanches: recent advances, potential, and limitations. Cold Reg. Sci. Technol. 121, 126–140.

Fee, D., Waxler, R., Assink, J., Gitterman, Y., Given, J., Coyne, J., Mialle, P., Garces, M., Drob, D., Kleinert, D., Hofstetter, R., Grenard, P., 2013. Overview of the 2009 and 2011 Sayarim Infrasound Calibration experiments. J. Geophys. Res. 118 (12), 6122–6143.

Gauer, P., Kern, M., Kristensen, K., Lied, K., Rammer, L., Schreiber, H., 2007. On pulsed Doppler radar measurements of avalanches and their implication to avalanche dynamics. Cold Reg. Sci. Technol. 50 (1–3), 55–71.

Hadden Jr., W.J., Pierce, A.D., 1981. Sound diffraction around screens and wedges for arbitrary point source locations. J. Acoust. Soc. America 69 (5), 1266–1276.

Havens, S., Marshall, H.P., Johnson, J.B., Nicholson, B., 2014. Calculating the velocity of a fast-moving snow avalanche using an infrasound array. Geophys. Res. Lett. 41 (17), 6191–6198.

Heck, M., Hammer, C., van Herwijnen, A., Schweizer, J., Fäh, D., 2018. Automatic detection of snow avalanches in continuous seismic data using hidden Markov models. Nat. Hazards Earth Syst. 18 (1), 383–396.

Heck, M., Hobiger, M., van Herwijnen, A., Schweizer, J., Fäh, D., 2019a. Localization of seismic events produced by avalanches using multiple signal classifications. Geophys. J. Int. 216 (1), 201–217.

Heck, M., van Herwijnen, A., Hammer, C., Hobiger, M., Schweizer, J., Fäh, D., 2019b. Automatic detection of avalanches using combining array classification and localization. Earth Surf. Dyn. 7 (2), 491–503.

Hendrikx, J., Dreier, L., Ulivieri, G., 2017. Evaluation of an Infrasound Detection System for Avalanches, Rogers Pass, Canada; Winter 2016–17. Report for McElhanney Consulting Services Ltd.

Hendrikx, J., Dreier, L., Ulivieri, G., Sanderson, J., Jones, A., Steinkogler, W., 2018. Evaluation of an infrasound detection system for avalanches in Rogers Pass, Canada. In: Fischer, J.-T. (Ed.), Proceedings ISSW 2018. International Snow Science Workshop, Innsbruck, Austria, pp. 171–175 7–12 October 2018.

Humstad, T., Soderblom, O., Ulivieri, G., Langeland, S., Dahle, H., 2016. Infrasound detection of avalanche in Grasdalen and Indreeidsdalen, Norway. In: Proceedings ISSW 2016. International Snow Science Workshop. Breckenridge CO, U.S.A, pp. 621–627 3–7 October 2016.

Johnson, J.B., Marshall, H.P., Loo, S.M., Nalli, B., Saurer, M., Havens, S., Colton, J., Anderson, J.F., 2018. Detection and tracking of snow avalanches in Little

Cottonwood Canyon, Utah using multiple small-aperture infrasound arrays. In: Fischer, J.-T. (Ed.), Proceedings ISSW 2018. International Snow Science Workshop, Innsbruck, Austria, 7–12 October 2018, pp. 616–620.

Kogelnig, A., Suriñach, E., Vilajosana, I., Hübl, J., Sovilla, B., Hiller, M., Dufour, F., 2011. On the complementariness of infrasound and seismic sensors for monitoring snow avalanches. Nat. Hazards Earth Syst. Sci. 11 (8), 2355–2370.

Kogelnig, A., Hübl, J., Suriñach, E., Vilajosana, I., McArdell, B.W., 2014. Infrasound produced by debris flow: propagation and frequency content evolution. Nat. Hazards 70 (3), 1713–1733.

Koschuch, R., 2018. 8 years experience in avalanche detection by using a Pulse Doppler Radar. In: Fischer, J.-T. (Ed.), Proceedings ISSW 2018. International Snow Science Workshop, Innsbruck, Austria, 7–12 October 2018, pp. 636–639.

Lacanna, G., Ripepe, M., 2013. Influence of near-source volcano topography on the acoustic wavefield and implication for source modeling. J. Volcanol. Geotherm. Res. 250, 9–18.

Lacroix, P., Grasso, J.R., Roulle, J., Giraud, G., Goetz, D., Morin, S., Helmstetter, A., 2012. Monitoring of snow avalanches using a seismic array: Location, speed estimation, and relationships to meteorological variables. J. Geophys. Res. Earth Surf. 117, F01034.

Marchetti, E., Ripepe, M., Ulivieri, G., Kogelnig, A., 2015. Infrasound array criteria for automatic detection and front velocity estimation of snow avalanches: towards a real-time early-warning system. Nat. Hazards Earth Syst. Sci. 15 (11), 2545–2555.

Marchetti, E., Lacanna, G., Le Pichon, A., Piccinini, D., Ripepe, M., 2016. Evidence of large Infrasonic Radiation Induced by Earthquake Interaction with Alluvial Sediments. Seismol. Res. Lett. 87 (3), 678–684.

McClung, D.M., Schaerer, P., 2006. The Avalanche Handbook. The Mountaineers Books, Seattle WA, U.S.A. (342 pp).

Mitterer, C., Schweizer, J., 2013. Analysis of the snow-atmosphere energy balance during wet-snow instabilities and implications for avalanche prediction. Cryosphere 7 (1), 205–216.

Naugolnykh, K., Bedard Jr., A.J., 2002. A model of the avalanche infrasonic radiation. IEEE International Geoscience and Remote Sensing Symposium 2, 871–872.

Persson, A., Venås, M., Humstad, T., Meier, L., 2018. Real-time radar avalanche detection of a large detection zone for road safety in Norway. In: Fischer, J.-T. (Ed.), Proceedings ISSW 2018. International Snow Science Workshop, Innsbruck, Austria, 7–12 October 2018, pp. 597–600.

Pertschy, S., Zweifel, B., Schweizer, J., Stucki, T., Gerber, M., Darms, G., 2016. ProTools and ProNXD: Record and manage avalanche activity. In: Koboltschnig, G. (Ed.), Extended Abstracts, 13th Congress INTERPRAEVENT 2016, 30 May-2 June 2016, Lucerne. Switzerland. International Research Society INTERPRAEVENT, Klagenfurt, Austria, pp. 144–145.

Ripepe, M., Marchetti, E., Ulivieri, G., 2007. Infrasonic monitoring at Stromboli volcano during the 2003 effusive eruption: Insights on the explosive and degassing process of an open conduit system. J. Geophys. Res. 112.

Schimmel, A., Hübl, J., Koschuch, R., Reiweger, I., 2017. Automatic detection of avalanches: evaluation of three different approaches. Nat. Hazards 87 (1), 83–102.

Schweizer, J., Alig, C., Mitterer, C., 2012. On indicator path avalanches for local avalanche forecasting. In: Proceedings ISSW 2012. International Snow Science Workshop, Anchorage AK, U.S.A., 16–21 September 2012, pp. 51–54.

Scott, E.D., Hayward, C.T., Kubichek, R.F., Hamann, J.C., Pierre, J.W., Comey, B., Mendenhall, T., 2007. Single and multiple sensor identification of avalanche-generated infrasound. Cold Reg. Sci. Technol. 47 (1–2), 159–170.

Steinkogler, W., Meier, L., Langeland, S., Wyssen, S., 2016. Operational radar and infrasound systems for avalanche detection. In: Proceedings ISSW 2016. International Snow Science Workshop, Breckenridge, Colorado, USA, 3–7 October 2016, pp. 309–315.

Steinkogler, W., Ulivieri, G., Vezzosi, S., Hendrikx, J., van Herwijnen, A., Humstad, T., 2018. Infrasound detection of avalanches: operational experience from 28 combined winter seasons and future developments. In: Fischer, J.-T. (Ed.), Proceedings ISSW 2018. International Snow Science Workshop, Innsbruck, Austria, 7–12 October 2018, pp. 621–626.

Thüring, T., Schoch, M., van Herwijnen, A., Schweizer, J., 2015. Robust snow avalanche detection using supervised machine learning with infrasonic sensor arrays. Cold Reg. Sci. Technol. 111, 60–66.

Ulivieri, G., Marchetti, E., Ripepe, M., Chiambretti, I., Rosa, G.D., Segor, V., 2011. Monitoring snow avalanches in Northwestern Italian Alps using an infrasound array. Cold Reg. Sci. Technol. 69 (2–3), 177–183.

Wilks, D.S., 2011. Statistical Methods in the Atmospheric Sciences. International Geophysics Series, 100. Academic Press, San Diego CA, U.S.A, pp. 467.